Annals of Nuclear Energy 186 (2023) 109773

Contents lists available at ScienceDirect

Annals of Nuclear Energy

journal homepage: www.elsevier.com/locate/anucene

Numerical prediction of turbulent flow and heat transfer in buoyancy-affected liquid metal flows

Andrea Pucciarelli [a,*], Afaque Shams [b,c], Nicola Forgione [a]

[a] Università di Pisa, Dipartimento di Ingegneria Civile e Industriale, Largo Lucio Lazzarino 2, 56122 Pisa, Italy
[b] Mechanical Engineering Department, King Fahd University of Petroleum & Minerals, Dhahran 31261, Saudi Arabia
[c] Interdisciplinary Research Center for Renewable Energy and Power Systems, King Fahd University of Petroleum & Minerals, Dhahran 31261, Saudi Arabia

ARTICLE INFO

Keywords:
Liquid metal
Heat transfer
RANS
DNS
Buoyancy

ABSTRACT

The present paper investigates the capabilities of some selected Reynolds-Averaged Navier Stokes (RANS) based turbulence models in reproducing liquid metals thermal hydraulics Direct Numerical Simulation (DNS) data. For this purpose, forced and mixed convection conditions, both addressing buoyancy-aided and buoyancy-opposed flow, are considered. The paper mainly focuses on velocity and temperature fields estimation, providing a comparison between the RANS and DNS computations. The capabilities of the turbulence models are discussed with the aim to highlight which ones provide the best predictions.

In particular, attention is paid to the approach adopted for the calculation of the turbulent heat flux contributions. Together with models assuming the commonly adopted Simple Gradient Diffusion Hypothesis (SGDH) approach and the Reynolds analogy, a model including the Algebraic Heat Flux Model (AHFM) approach is considered. While being a practical and robust approach to deal with turbulent heat fluxes, the SGDH approach shows intrinsic limitation in dealing with liquid metal thermal hydraulics, mainly because of their low-Prandtl number. The adoption of a more advanced AHFM method may instead relevantly improve the quality of the obtained predictions.

The obtained results show that the selected model adopting the AHFM method provides definitively better predictions of the addressed phenomena with respect to the ones considering the SGDH approach. While some discrepancies are still observed for the velocity fields, the temperature fields are captured very well, suggesting a clear superiority of the AHFM model. The present paper thus provides further validation and supports the use of AHFM as a valuable tool to predict turbulent heat fluxes.

1. Introduction

Liquid metals thermal-hydraulics represents an interesting topic for several industrial and engineering applications. In the nuclear field, liquid lead and sodium were considered for two plants concepts included by the GIF consortium (GIF, 2020) among the accepted proposals for the fourth generation of the nuclear power plants, namely the LFR (Lead Fast Reactor) and the SFR (Sodium Fast Reactor). Among the advantages in the adoption of such working fluids are the extremely large heat capacity, the good thermal conductivity and heat transfer capabilities and the low scattering and absorption cross sections. Several EU projects supported (e.g., MYRTE; SESAME; THINS) and presently support (e.g., PATRICIA, ANSELMUS) the development of Liquid Metal Fast Breeder Reactors (LMFBRs), providing room for further liquid metal thermal-hydraulics experimental and numerical investigations and understanding (Roelofs, 2019).

Unlike other fluids adopted in industrial applications, liquid metals exhibit very small Prandtl numbers, in the range of 0.004–0.04. This occurrence strongly impacts heat transfer to liquid metals: thermal boundary layers turn, in fact, to be relevantly larger than the ones experienced by fluids reporting an almost unitary Prandtl number. Therefore, the numerical tools needed to simulate the involved phenomena may require relevant changes, tuning, or the development of advanced turbulence modelling techniques (Shams, 2019).

Concerning applications considering real size plants and facilities adopting the RANS approach, several research groups assumed that as a first approximation, the Reynolds analogy may still be considered suitable: a Simple Gradient Diffusion Hypothesis (SGDH) and a constant

* Corresponding author.
E-mail address: andrea.pucciarelli@unipi.it (A. Pucciarelli).

https://doi.org/10.1016/j.anucene.2023.109773
Received 17 November 2022; Received in revised form 16 January 2023; Accepted 20 February 2023
Available online 27 February 2023

value of the Pr_{tur} is thus considered. Numerical applications involving fluids exhibiting a unitary Prandtl number showed that considering a Pr_{tur} in the range of 0.85–0.9 is sufficient to achieve a good level of correspondence with experimental data. For liquid metals, instead, experimental investigations suggest that Pr_{tur} values up to 3.5 can be observed (NEA, 2015): concerning numerical applications, a $Pr_{tur} = 1.5$ was for example considered in several works performed at the University of Pisa (Buzzi et al., 2020; Galleni et al., 2020) involving LBE thermal hydraulics. This is of course a strong simplifying assumption which, on one side, allows adopting robust and well-known turbulence models but, on the other hand, shows several limitations when it is asked to reproduce turbulent flows in complex geometries (see e.g. wire-wrapped rod bundles). Obvious limitations are also reported for mixed and natural circulation conditions, whose investigation is required to assess the capabilities of the proposed nuclear plant passive cooling systems (Shams et al., 2019a,b).

Conversely, as highlighted by high fidelity calculations, in order to achieve an improved description of the involved heat transfer phenomena, advanced numerical tools for the calculation of the turbulent heat flux contributions may be required (Bartosiewicz, 2021). Marocco and Garita (2018) performed a LES analysis of a fluid exhibiting a Pr = 0.026 in a vertical concentric annulus. Shams et al. (2018) performed an LES of liquid lead, with the Pr = 0.016, in a loosely spaced rod bundle flow. Turbulent Prandtl number distributions were investigated, suggesting that, especially for mixed convection cases, the SGDH approach seems not sufficient to represent the addressed phenomena. Pucciarelli (2021), performed a LES calculation addressing LBE flowing in a single rod wire wrapped channel, concluding that at least a Generalized Gradient Diffusion Hypothesis (GGDH) may be required in order to better predict the turbulent heat flux.

DNS calculations addressing both forced and mixed convection for low Prandtl fluids were recently published as well. In their work, Tiselj and Cizelj (2012) investigated the importance of temperature fluctuations on conjugated heat transfer problems. Shams et al. (2018) performed a quasi-DNS computation of an infinite wire-wrapped fuel assembly for an LBE coolant flow. Additionally, within the framework of EU SESAME and MYRTE, an extensive effort was put forward to generate reference database for liquid metal flows, reader are referred to see (Shams et al., 2019a). De Santis et al. (2018) performed DNS calculations addressing forced and mixed flow in a plane channel for fluids with Pr = 1, 0.1 and 0.01. Comparisons with RANS analyses calculation were performed highlighting the limits of the SGDH approach while observing interesting capabilities for the Algebraic Heat Flux Model (AHFM) for the calculation of the turbulent heat flux components. Moreover, Guo et al. (2020) performed DNS for liquid metal flows in a channel by varying the Richardson number to study the influence of buoyancy. This work was later reproduced with the use of RANS models to highlight the shortcomings of SGDH approach. Shams et al. (2020) performed a DNS of low-Pr number flow analyses in a tightly spaced bare-rod bundle case to further assess different RANS models. More recently, Guo and Prasser (2022) performed a DNS calculation for a fluid exhibiting Pr = 0.025 flowing upwards in a vertical plane channel. Buoyancy-aided and buoyancy-opposed flows were investigated reporting interesting velocity and temperature distributions valuable for a further validation of the available modelling tools for RANS approaches.

The AHFM models proposed in Kenjeres et al. (2005); Shams et al. (2014); Shams and De Santis (2019) are the most advanced modelling techniques for the calculation of the turbulent heat flux contributions. The AHFM approach, proposed by Launder (1988), is a simplification of the turbulent heat flux transport equation, its application requires the calculation of the temperature variance distribution, thus requiring the solution of at least an additional dedicated transport equation. In literature, several authors suggested tuned sets of parameters in order to achieve a better representation of the addressed phenomena. The model proved interesting capabilities and flexibility since it was successfully adopted to improve heat transfer predictions in different industrial applications, straddling from air flows (see e.g. Kenjeres et al., 2005), liquid metals (see e.g. Shams et al., 2014; Shams and De Santis, 2019) to supercritical fluids (see e.g. Pucciarelli and Ambrosini, 2018; Zhang et al., 2012). In the framework of severe accidents scenarios, particularly in the in-vessel melt retention case, the resulting Rayleigh number (Ra) of the corium pool is significantly high. To that respect, Shams (Shams, 2018) extended the AHFM formulation (Shams et al., 2014) to deal with such high Rayleigh numbers. It is worth mentioning that, overall, the base model was still the same as used in Shams et al. (2014), however, a new correlation was proposed. This correlation was in addition to already proposed Shams correlations for the model co-efficient (C_{t1}) in Shams et al. (2014). Later on, this extended AHFM formulation was tested for high Ra and different Richardson (Ri) number flows and have shown significant improvements over the initial proposed AHFM-NRG formulation, for details readers are referred to Shams (2018) and Shams (2019). It is worth highlighting that merely the use of AHFM-NRG doesn't guarantee the use of advanced turbulent heat flux modelling. Therefore, it must be highlighted that without the use of Shams correlation, the model is bound to fail. This is mainly because the proposed Shams correlations in Shams et al. (2014) and Shams (2018) have been calibrated for a wide range of flow applications and will provide significant improvements over the default model co-efficients. Therefore, in this study, to avoid all the ambiguity, this model will be referred as AHFM-SC (SC = Shams correlation). This issue has been recently highlighted in Shams (2023). Nonetheless, all these aforementioned AHFM formulations rely on a linear low-Reynolds $k - \varepsilon$ model for the closure of the turbulent momentum flux. This, at times hinder the possibility to obtain accurate results for complex geometries. To overcome such challenges, the aforementioned Shams correlations were extended to be used together with a low-Reynolds second moment closure, that is Reynolds Stress Model based on Elliptical Blending (RSM-EB), and was first introduced in Shams and De Santis (2019).

The rich database provided by Guo and Prasser (2022) is considered in the present paper as a useful mean to further investigate the capabilities of RANS turbulence models in predicting liquid metals thermal-hydraulics phenomena involving forced and mixed convection conditions. Commonly used and well-known turbulence models adopting a SGDH approach for the turbulent heat flux calculation are firstly considered, trying to evaluate their capabilities in reproducing the addressed operating conditions. The AHFM-SC model (Shams, 2023), adopting the AHFM for the calculation of the turbulent heat flux contributions is also taken into account. The performed analyses reports that relevant improvement in the prediction of both velocity and temperature fields may be achieved adopting the AHFM-SC model, thus supporting the need of advanced tools to achieve a suitable prediction of the addressed phenomena.

2. Considered operating conditions and CFD domain

As anticipated in the previous section, the present work aims at reproducing the DNS data by Guo and Prasser (2022) by means of RANS calculations, chiefly focusing on the application of the AFHM-SC model to be introduced in section 3.

Guo and Prasser (2022) performed DNS calculations investigating the behaviour of a low-Prandtl number fluid (Pr = 0.025, i.e., values in the range of liquid metals applications) in a vertical channel. Both forced convection and buoyancy-affected conditions were considered. The considered geometry is reported in Fig. 1: it consists of a vertical plane channel of width 2δ. The liquid metal flows upwards: a constant mass flow rate is assumed, and different constant temperatures are imposed on the channel walls. This way, a hot and a cold wall can be identified. The considered geometry, depending on the imposed temperature and mass flow conditions, identifying forced or mixed flow conditions, may imply the occurrence of a buoyancy-aided and a buoyancy-opposed regions in correspondence of the hot and cold wall, respectively. This

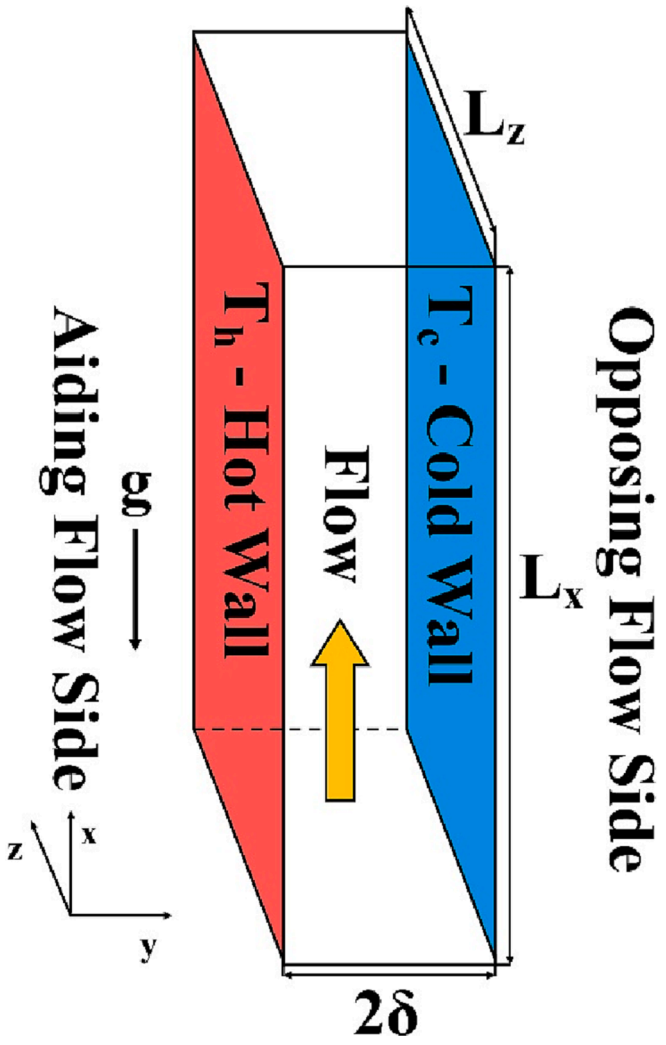

Fig. 1. Coordinate System and Flow Geometry.

setting thus provides a very interesting environment for the numerical investigations.

In similarity with the vast majority of DNS literature, in their work, Guo and Prasser (2022) provided the geometrical parameters and the operating conditions of the addressed domain in a dimensionless form. Concerning the operating conditions, a bulk Reynolds number of 4667 was considered: four test cases, each one investigating a different Richardson number scenario (Ri = 0 i.e. Forced Convection, Ri = 0.25, Ri = 0.5 and Ri = 1) were addressed. The adopted dimensionless approach grants a certain level of universality to the obtained results, which are thus suitable for any flow and geometrical conditions fulfilling the considered setting. On the other hand, the RANS approach considered in the present work, requires instead a dimensional approach: the conditions investigated by Guo and Prasser (2022) must thus be translated in a dimensional form.

This procedure required a series of assumptions. First, a suitable combination of the liquid metal and of the operating conditions had to be found in order to both achieve the desired Pr = 0.025 while also facing velocity and temperature distributions that may have a physical basis and a clear interest for engineering applications.

A good compromise was found in the LBE properties at 547 K reported in Table 1. The considered set of properties can thus be adopted in order to derive a correspondent dimensional form of the boundary conditions assumed by Guo and Prasser (2022) in their work. The obtained geometrical, flow and boundary conditions are reported in Table 2. As it can be observed, a small temperature range is foreseen also

Table 1
Considered LBE operating temperature conditions.

T [K]	ρ [kg/m^3]	μ [Pa s]	Cp [J/kgK]	k [W/mK]	β [1/K]	Pr [−]
547.0	10357.73	0.001961	145.46	11.44	0.00012	0.0249

Table 2
Considered LBE operating temperature conditions.

Re [-]	Ri [-]	δ [m]	v_{in} [m/s]	T_h[K]	T_c[K]	Gr [−]
4667	0	0.0175	0.02524	547.0	547.0	0
4667	0.25	0.0175	0.02524	548.85	545.14	$0.544 \bullet 10^7$
4667	0.50	0.0175	0.02524	550.71	543.28	$1.089 \bullet 10^7$
4667	1.00	0.0175	0.02524	554.43	539.56	$2.178 \bullet 10^7$

for the conditions involving the largest buoyancy forces. As a consequence, also owing to the limited changes in the fluid properties experienced by LBE in the very same range, a constant properties fluid can be considered in the numerical calculations. Buoyancy forces are taken into account by introducing the well-known Boussinesq approximation for buoyancy:

$$\vec{f_g} = \rho_{ref} \bullet \vec{g} \bullet \beta\left(T_{ref} - T\right) \tag{1}$$

where $\vec{f_g}$ is the volumetric buoyancy force and ρ_{ref} and T_{ref} are respectively the reference density and temperature which, in this case, are assumed to be the ones of LBE at the considered temperature of 547.0. The approximation is valid if $\beta\left(T_{ref} - T\right) \ll 1$, which is true for all the considered operating conditions.

Moving to the considered CFD domain, simplifying assumption were introduced with respect to the DNS domain taken into account by Guo and Prasser (2022). In particular, owing to the considered geometry, RANS calculations allow for the analysis of a 2D domain, thus neglecting the z-direction. Also, the addressed DNS calculations took into account periodic boundary conditions both in the streamwise (i.e. inlet–outlet) and spanwise (i.e. z) directions. The flow exiting the domain at the outlet section was thus again imposed as an inlet condition; a source term balancing the pressure drops experienced in the considered domain was also included. These assumptions allowed for reaching fully developed conditions while also limiting the computational cost.

In the RANS domain developed in the frame of the present work, owing to the assumed bi-dimensional geometry, no periodic conditions had to be imposed for the spanwise direction, which indeed does not exist anymore. Concerning the considered streamwise length, since the adopted approach requires a limited computational cost, a 10 m long channel was assumed. This prevents the need of including periodic interfaces and compensating source terms while also assuring, at least for the addressed operating conditions, reaching a fully developed flow well before the outlet section. The addressed geometry and flow conditions reassure that the adopted simplifications do not affect the final results. In fact, even a 3D domain, adopting the RANS approach, would have deemed the spanwise structures to be null. In addition, the considered pipe length also assures that a full developed flow is achieved. The results provided in the next section are collected right in the middle of the pipe, the very same trends can be observed both slightly upstream and up to the pipe outlet section thus confirming the suitability of the adopted strategy.

The spatial discretization was performed creating a nodalization exhibiting a uniform mesh size in the streamwise direction of the size 0.01 m. In addition, in accordance with the LowRe approach considered for all the addressed turbulence models, a refinement in the vicinity of the walls had to be included in order to assure to fulfil the requirement of $y^+ < 1$ for all the considered conditions for the first cell next to the wall. Several mesh sizes were considered for the mesh independence analysis,

mainly focusing on the relevant quantities considered for the comparison with the Guo and Prasser DNS data i.e. velocities and temperature fields but also turbulent quantities. The nodalization considered in the frame of the present work reports a final element count of about 1.1 • 10^5 cells, thus allowing for a relatively less computational demand while assuring the reliability of the obtained results.

3. Adopted turbulence models

In the present work, the capabilities of an advanced turbulent heat flux model, the AHFM-SC model, are assessed against the Guo and Prasser (2022) DNS data. A comparison with the predictions provided by other available well-known turbulence models is performed as well. These selected models, all adopting the Simple Gradient Diffusion Hypothesis for the sake of calculating the turbulent heat fluxes, are: the Lien k-ε model (Lien et al., 1996), the SST k-ω model (Menter, 1994) and the V2F model (Durbin, 1996). The reader is referred to the cited papers for a deeper description of the turbulence models. It is worth mentioning that the AHFM-SC is briefly discussed here.

The AHFM-SC model (see e.g. Shams et al., 2014 for its first application) was developed to purposely deal with non-unity Prandtl number fluids, particularly the liquid metal flows. Owing to the limits reported by the commonly used eddy diffusivity approach, the model adopts the AHFM formulation for the estimation of the turbulent heat flux contributions. The AHFM is an advanced formulation allowing introducing the intrinsic anisotropic nature of turbulence in the RANS energy equation. It was derived by Launder (1988) as a simplification of the turbulent heat flux transport equation and later updated by other authors. The transport equations proposed in Kenjeres et al. (2005) are maintained in the AHFM-SC model too. In the AHFM-SC model, the turbulent heat flux formulation is given as:

$$\overline{u_i't'} = -C_{t0}\frac{k}{\varepsilon}\left(C_{t1}\overline{u_i'u_j'}\frac{\partial T}{\partial x_j} + C_{t2}\overline{u_j't'}\frac{\partial U_i}{\partial x_j} + C_{t3}\beta g\overline{\theta'^2}\right) + C_{t4}a_{ij}\overline{u_j't'} \quad (1)$$

where $a_{ij} = \frac{\overline{u_i'u_j'}}{k} - \frac{2}{3}\delta_{ij}$. Here, the first term in the AHFM relation ($C_{t1}\overline{u_i'u_j'}\frac{\partial T}{\partial x_j}$) consists of the Generalized Gradient Diffusion Hypothesis (GGDH) and represents the anisotropic nature of eddy-diffusivity and plays the most relevant role in forced convection conditions. The second term ($C_{t2}\overline{u_j't'}\frac{\partial U_i}{\partial x_j}$) takes into account the mutual influence occurring between the turbulent heat flux components and helps improving the prediction for intrinsically 3D conditions (see e.g. free jets, Launder, 1988). The third component ($C_{t3}\beta g\overline{\theta'^2}$) is to be connected instead to the buoyancy effects. The last term relates instead to the Reynolds stress anisotropy tensor. Each contribution is multiplied by a coefficient, providing a suitable weighting of the contribution itself in the global balance of the turbulent heat flux. It is here remarked that, in order to comply with numerical stability issues, the C_{t4} parameter is here set to zero, in similarity with previous works (see e.g. Shams and De Santis, 2019).

Together with the Ct_0 - Ct_4 set of parameters, this model also requires the estimation of the temperature variance $\overline{\theta'^2}$ field: an additional transport equation is thus needed. The transport equation for $\overline{\theta'^2}$ can be derived from theory (Kenjeres et al., 2005) and it is:

$$\frac{D\rho\overline{\theta'^2}}{Dt} = 2P_\theta - 2\rho\varepsilon_\theta + \frac{\partial}{\partial x_j}\left[\left(\frac{\lambda}{c_p} + \frac{\mu_t}{\sigma_{\theta'^2}}\right)\frac{\partial\overline{\theta'^2}}{\partial x_j}\right] \quad (2)$$

where $P_\theta = \rho\overline{u_i't'}\frac{\partial T}{\partial x_i}$. Some models also include an equation for ε_θ, thus opting for a four-equation turbulence model. Following other experiences available in literature, the AHFM-SC model adopts instead an algebraic relation to calculate ε_θ; a constant thermal to mechanical time scale ratio R = 0.5 (Hanjalic et al., 1996) is in fact assumed.

R is defined as:

$$R = \frac{\tau_\theta}{\tau_m} \quad (3)$$

where $\tau_\theta = \frac{\overline{\theta'^2}}{2\varepsilon_\theta}$ and $\tau_m = \frac{k}{\varepsilon}$.

The system of equations thus becomes a closed problem. This model has been implemented in STAR-CCM+ (Simcenter, 2018) in the frame of the THINS project (Shams et al., 2014). In the STAR-CCM + environment, it can be selected in association with the Lien k-ε model and it is termed as Temperature Flux Model.

The parameters of the model originally proposed by Shams et al. (2014) were later updated in order to better address both forced and mixed/natural circulation conditions. The latest set of parameters also considered in the present work, is reported in Table 3,

where:

$$C_{t1} = 0.053\ln(RePr) - 0.27, validforRePr > 180 \quad (4)$$

$$C_{t3} = -4.5 \bullet 10^{-9}(\log(RaPr))^7 + 2.5, validfor1 < RaPr < 10^{17} \quad (5)$$

The introduction of the AHFM model increases the computational cost of the model; an additional transport equation must in fact be solved for each cell of the domain. Nevertheless, the claimed improved modelling capabilities should provide a relevant edge in comparison to other models. This should be particularly true for the addressed DNS data. In fact, since mixed/natural circulation conditions are involved, the eddy diffusivity approach adopted by the common turbulence models is likely deemed to fail. The AHFM-SC model is instead expected to provide better estimations, allowing to capture the fundamental aspects of the addressed operating conditions.

4. Obtained results

In the present section, the results provided by the RANS calculations obtained in the frame of this work are compared with the addressed DNS results by Guo and Prasser (2022). The comparison is performed on the basis of some of the dimensionless parameters highlighted by Guo and Prasser in their work defined hereinafter.

In all the presented figures, the quantity y, representing the dimensionless coordinate along the width direction defined as $y = \frac{y_{rs}}{2\delta}$ is taken into account for the x-axis. Here, y_{rs} is the reference system coordinate along the width direction, whose origin is positioned right in the middle of the channel: as a consequence, the region $-0.5 < y < 0$ represents the buoyancy-aided side while the $0 < y < 0.5$ region corresponds to the buoyancy-opposed side. The velocity is made dimensionless by considering the ratio $\overline{u^+} = \frac{\overline{u}}{u_\tau}$ where $\overline{u}$ is the local mean axial velocity while u_τ represents the shear stress velocity of the referred wall. As a consequence, owing to the different u_τ value considered for each side of the channel, relevantly different values and, in particular, a jump in correspondence of the mid-section are to be expected in the $\overline{u^+}$ distribution. Eventually, the dimensionless temperature is defined as $\overline{T^+} = \frac{\overline{T} - T_c}{T_h - T_c}$ where $\overline{T}$ is the local mean temperature, and T_c and T_h are the temperatures imposed at the cold and hot wall, respectively. As a consequence, $\overline{T^+}$ spans between 0 on the cold wall and 1 in correspondence of the hot wall.

Fig. 2 reports the comparison between the DNS reference data and the RANS calculations performed in the present work for the addressed forced convection case. As it can be observed, all the selected models can predict the velocity distribution in a quite good manner. Some discrepancies are of course to be expected; all the considered models in fact

Table 3
AHFM-SC parameters for the AHFM correlation.

C_{t0}	C_{t1}	C_{t2}	C_{t3}	C_{t4}	R
0.25	Eq. 3	0.6	Eq. 4	0	0.5

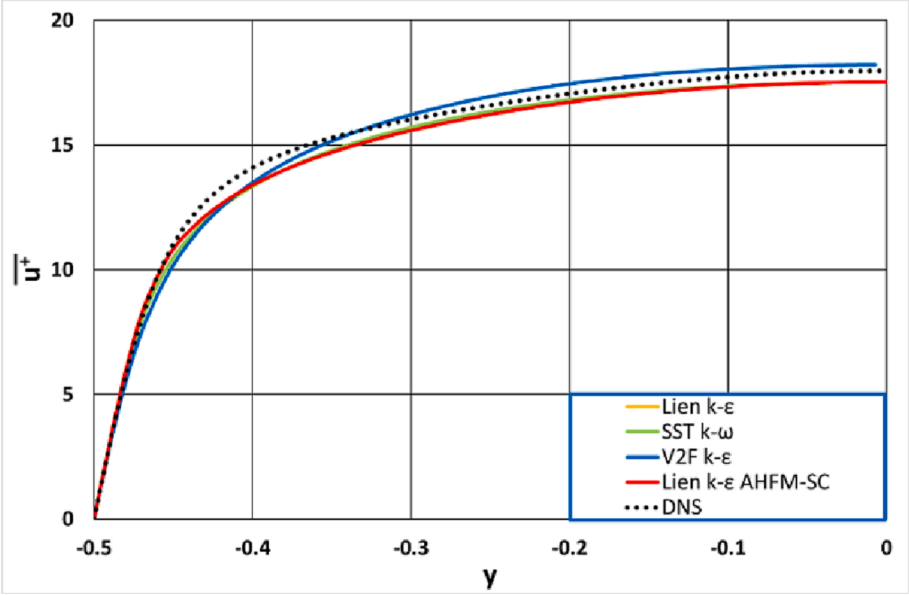

Fig. 2. DNS and RANS dimensionless velocity distributions for the Forced Convection Case.

underpredict the DNS velocity distribution in the region y = -0.4. Though, the global phenomenon was correctly captured, and the observed differences are sufficiently small to claim success for all the considered turbulence models.

Figs. 3 and 4 report instead the dimensionless velocity trends for the operating conditions considering a Richardson number Ri = 0.25: as it can be observed, buoyancy forces start playing a significant role on the observed phenomena. Both the velocity trends underwent deformation because of buoyancy: on the aiding flow side, velocities increase in the vicinity of the wall while on the opposing flow side the flow is slowed. Owing to the slower involved velocities, the shear velocity on the opposing flow side is smaller too, thus implying larger values of the dimensionless velocity $\overline{u^+}$. Concerning the RANS predictions, for the aiding flow side almost all the turbulence models managed to reproduce the DNS trend, the best results were provided by the SST k-ω and the AHFM-SC models. Poor results were instead observed for the opposing flow side, where only the AHFM-SC manages to provide a suitable prediction of the DNS data; the other considered models instead, relevantly over and underestimated the reference data. For the temperature field reported in Fig. 5, instead, the best prediction is again reported by the AHFM-SC model. In fact, only AHFM-SC manages to predict the symmetrical behaviour reported by the DNS data, predicting the correct

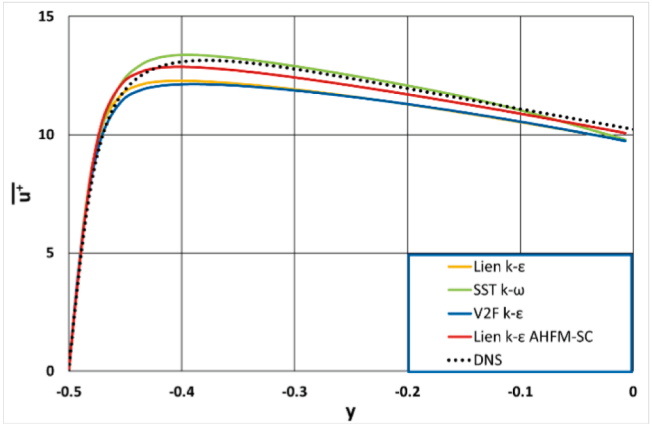

Fig. 3. DNS and RANS dimensionless velocity distributions for the aiding flow side for the Ri = 0.25 Case.

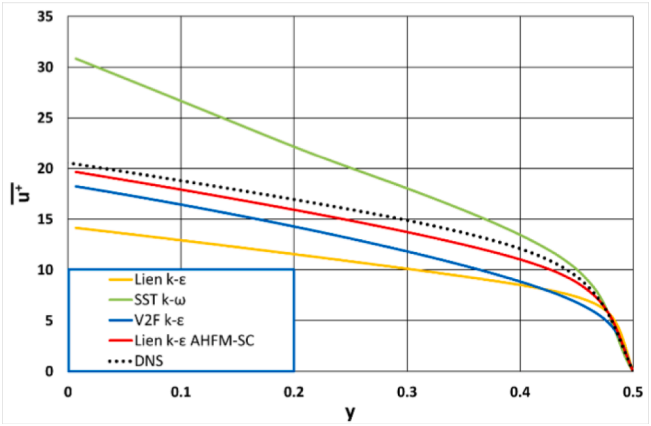

Fig. 4. DNS and RANS dimensionless velocity distributions for the opposing flow side for the Ri = 0.25 Case.

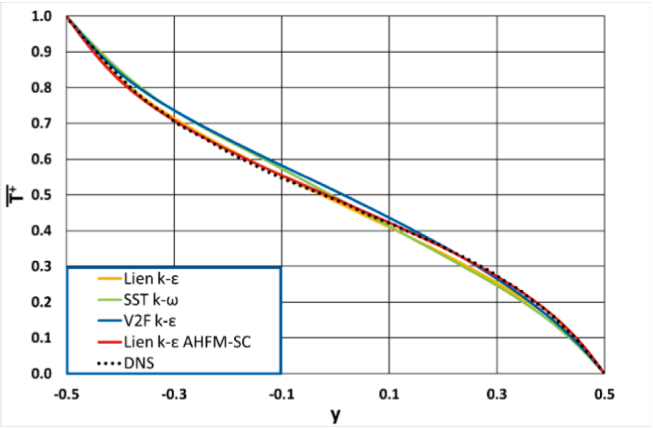

Fig. 5. DNS and RANS dimensionless temperature distributions for the Ri = 0.25 Case.

temperature distributions on both the heated walls. The Lien k-ε model manages instead to well predict the hot wall region while behaving poorly on the other side; on the other hand, the V2F model manages to provide a good estimation of the cold side but strongly overpredicts the temperature distribution on the hot side and in the middle of the channel. The capabilities of the AHFM-SC model in predicting the temperature field are better highlighted in Fig. 6, which reports the difference between the DNS and RANS results for the considered models at each y position. As it can be observed, AHFM-SC not only reports the best qualitative trend, but it also provides the smallest errors, which are usually well inside the ± 0.01 range. Definitively larger values are instead reported by the other considered models. As a final remark on this case, it can be observed that, even for these conditions, in which buoyancy plays a limited role, the simple gradient approach adopted by the Lien k-ε, SST k-ω and V2F models seems no more sufficient to deal with the involved phenomena. The DNS trends are instead well reproduced when including the AHFM-SC model, which allows for a better estimation of the turbulent heat flux contributions.

Figs. 7 and 8 report the comparisons of the velocity distribution trends predicted by the DNS by Guo and Prasser (2022) and the presently considered RANS turbulence models for the operating conditions assuming Ri = 0.50. As it can be observed, on the aiding flow side, the SST k-ω model provides the best predictions, being almost superimposed to the DNS data for several y locations. Small underestimations are predicted by the AHFM-SC model while larger discrepancies are instead reported by the Lien k-ε and the V2F models. The situation changes for the opposing flow region: here the AHFM-SC undoubtedly provides the best estimation; the Lien k-ε model and the V2F model provide again the worst results. The prediction provided by the SST k-ω model must instead be highlighted, since it reports a strong overestimation of the buoyancy forces: the velocity trends in fact show a reverse flow in the vicinity of the cold wall, something that is not predicted yet by the DNS calculations. The large $\overline{u^+}$ values on the opposing flow side are again due to very small u_τ values calculated in correspondence of the cold wall that, as predicted by the SST k-ω model, may be very close to a situation in which reverse flow may be experienced. Moving to the temperature distributions reported in Fig. 9, the good capabilities of the AHFM-SC model are again confirmed. AHFM-SC manages again to reproduce the DNS trend along the width direction in a suitable way, achieving superimposition at several locations. Unfortunately, the other considered models behave poorly. With the increasing of the buoyancy effects with respect to the Ri = 0.25 case, the simple gradient approach shows more and more limitations. Heat transfer is generally overestimated in opposing flow side while at least the Lien k-ε model seems providing a sufficiently close prediction for the aiding flow side. Concerning the symmetry of the profile, only the AHFM-SC model shows again a trend close to the DNS reference one, all the other considered models, instead, fail in achieving the desired symmetry. Fig. 10 helps in achieving a quantitative estimation of the discrepancies between the DNS and RANS temperature distributions. AHFM-SC, again, manages to keep the error below the ± 0.02 range while the other considered models definitively show poorer capabilities.

Eventually, from Fig. 11 to 14, the Ri = 1.00 case is investigated.

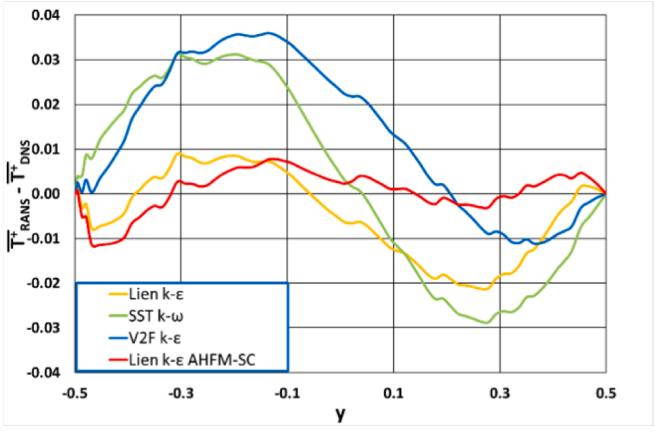

Fig. 6. RANS calculations offset for the dimensionless temperature distributions for the Ri = 0.25 Case.

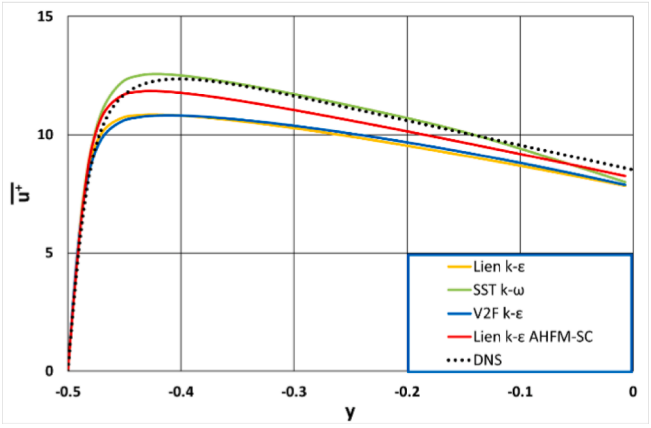

Fig. 7. DNS and RANS dimensionless velocity distributions for the aiding flow side for the Ri = 0.50 Case.

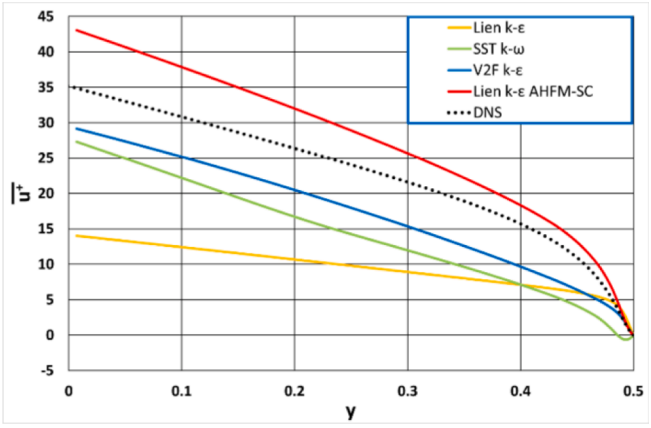

Fig. 8. DNS and RANS dimensionless velocity distributions for the opposing flow side for the Ri = 0.50 Case.

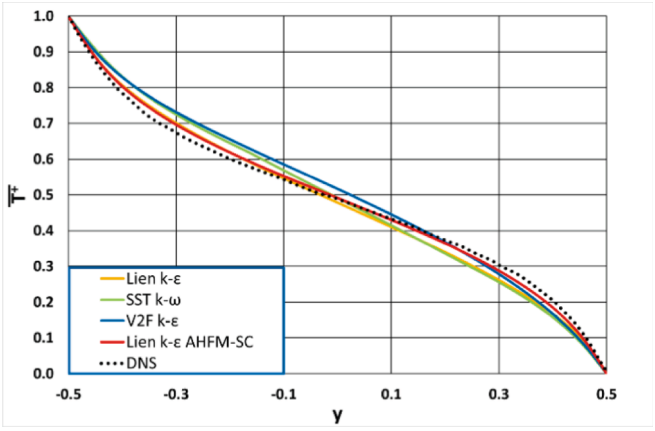

Fig. 9. DNS and RANS dimensionless temperature distributions for the Ri = 0.50 Case.

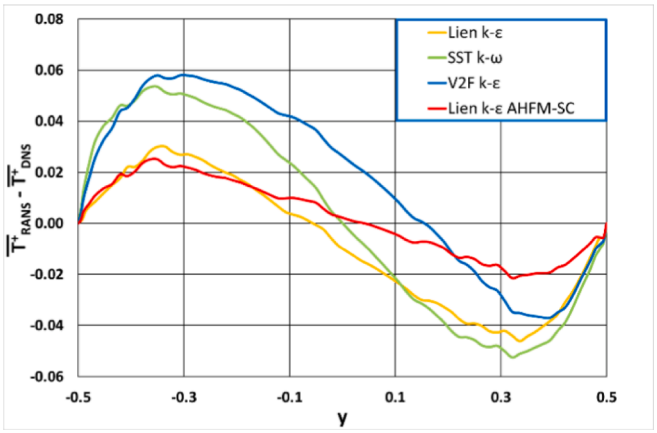

Fig. 10. RANS calculations offset for the dimensionless temperature distributions for the Ri = 0.50 Case.

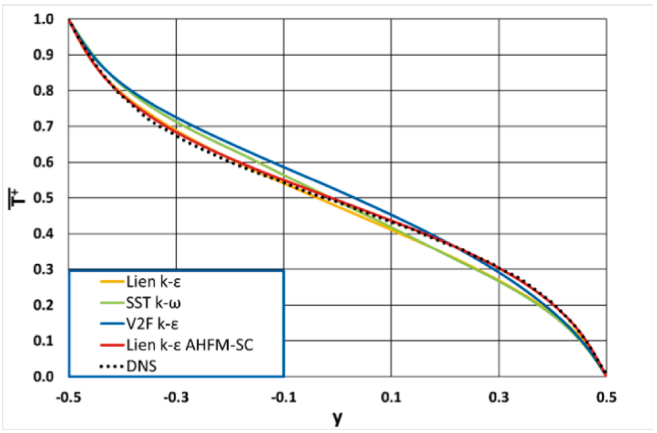

Fig. 13. DNS and RANS dimensionless temperature distributions for the Ri = 1.00 Case.

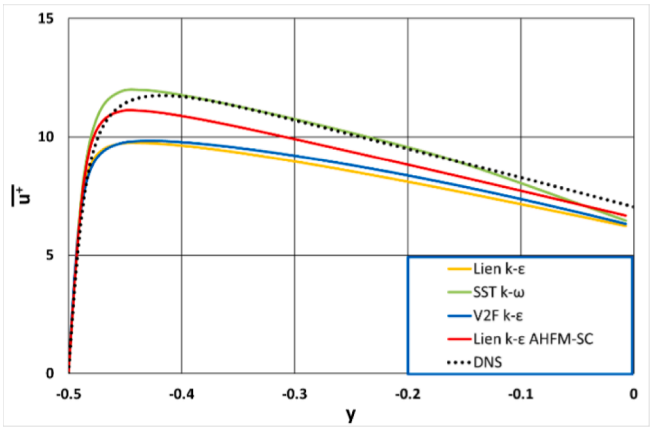

Fig. 11. DNS and RANS dimensionless velocity distributions for the aiding flow side for the Ri = 1.00 Case.

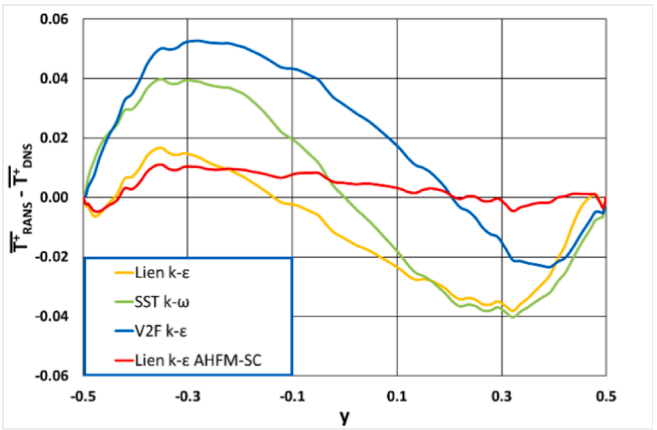

Fig. 14. RANS calculations offset for the dimensionless temperature distributions for the Ri = 1.00 Case.

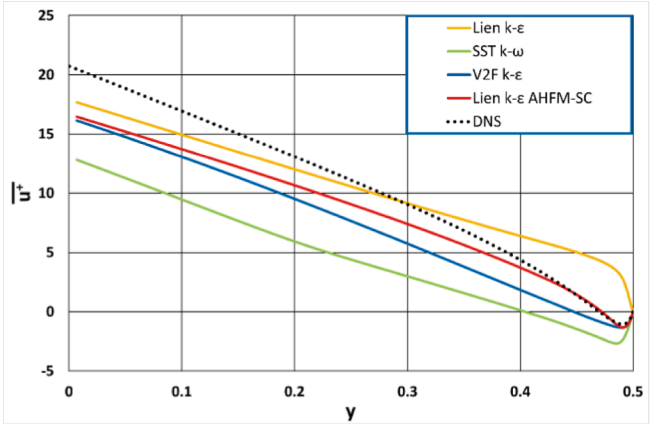

Fig. 12. DNS and RANS dimensionless velocity distributions for the opposing flow side for the Ri = 1.00 Case.

Fig. 11 shows the comparison for the aiding flow side; as expected, the best predictions are again the ones provided by the SST k-ω and the AHFM-SC models; the Lien k-ε and V2F models keep underestimating the buoyancy forces contributions. Moving to the opposing flow side, interestingly, in this case DNS predicts a reverse flow in the vicinity of the wall. AHFM-SC provides a very good prediction, the DNS and RANS data are indeed almost superimposed in the region close to the wall, while the reference distribution is slightly underestimated as the central region of the channel is approached. The SST k-ω model, which already predicted reverse flow for the case Ri = 0.50, again overestimates the buoyancy forces, predicting larger velocity values in the vicinity of the wall; on the other hand, buoyancy forces are strongly underestimated by the Lien k-ε model which does not predict any reverse flow. Fig. 13 reports the comparisons between the DNS and RANS predictions for the temperature distribution inside the channel. At this stage, only the AHFM-SC model managed to provide a suitable representation of the DNS data, reporting a very good matching for almost all the locations along the width direction. The other models, instead, definitively fail at both sides, reporting somehow more difficulties for the opposing flow side, something acting coherently with the observed discrepancies for the dimensionless velocity trends. With buoyancy effects becoming more and more relevant with respect to other cases, the limits of the models adopting the simple gradient approach become clearer, larger discrepancies with respect to the DNS reference data are experienced and symmetrical temperature distribution trends were not achieved. On the other hand, AHFM-SC manages to reproduce the expected symmetry of the temperature profile, supporting the reliability of the adopted model. Fig. 14 reports the distribution of the discrepancies between the DNS and RANS calculations: only the AHFM-SC model manages to provide estimations in the ± 0.01 range; failure is instead reported by the other models, reporting very large values either for the hot or cold side depending on the selected one.

The conditions addressing the Ri = 1 case are here more deeply analysed in a dimensional form trying to understand the reasons of the

improved prediction of the DNS data reported by the AHFM-SC model. The Lien k-ε model is considered being considered for the comparison being the basis of the AHFM-SC model, its application in association with the Yap correction (Yap, 1987) in the ε equation is considered, since it is adopted in the AHMD-SC model, too.

Fig. 15 reports about the dimensional velocity trends predicted by the considered models. As it can be observed the Yap correction seems very important to predict a better estimation of the velocity field. As observed before, the original Lien k-ε model cannot predict the reverse flow occurring in correspondence of the opposing flow side. The activation of the Yap correction seems instead sufficient to provide an improved prediction of the DNS data, reporting a trend very close to the one provided by the AHFM-SC model.

The Yap correction improves the prediction also for what concerns the temperature field. As reported in Fig. 16, the Yap correction prediction is close to the trend predicted by AHFM-SC in correspondence of the opposing flow side, and consequently closer to DNS than the original Lien k-ε model. Nevertheless, the prediction slightly impairs for the aided flow side. AHFM-SC consequently still performs better.

Figs. 17 and 18 report about turbulent quantities. The AHFM-SC introduces the buoyancy contribution in the turbulent kinetic balance equation (G_k); nevertheless, the impact of buoyancy production seems very limited, especially near the aided flow side, where the production due to shear (P_k) is very large. The effects on the turbulent kinetic energy distribution are indeed very small, and all the selected models predict very similar trends.

What instead turns to be relevantly different is the distribution of the Turbulent Heat Flux (THF) along the y-direction, the leading one for the addressed phenomenon. As it can be observed in Fig. 19, both the original Lien k-ε model and the one accounting for the Yap correction strongly overestimates the THF value predicted by AHFM-SC, especially in the bulk region. According to these models, here THF is overwhelming with respect to molecular transport; AHFM-SC predicts instead the THF to be comparable with molecular heat flux. This is thus the key feature leading to the discrepancies observed in the temperature distribution. The comparison with DNS data suggests that the AHFM-SC approach is the best one among the considered models, and the here reported analysis connects the observed improvements directly to the use of AHFM, providing a better estimation of THF with respect to the SGDH approach adopted by other models.

5. Conclusions

The present paper investigated the capabilities of four selected turbulence models in dealing with forced and mixed convection conditions involving liquid metals. The DNS data by Guo and Prasser (2022) for a Pr = 0.025 fluid flowing upwards in a vertical plane channel were taken as reference, and four cases addressing the increasing relevance of the buoyancy forces were investigated.

The analyses showed that, for the forced convection conditions, all the selected models managed to provide a suitable prediction of the DNS trends. Moving to mixed convection conditions, the selected models adopting the simple gradient approach for the sake of calculating the turbulent heat flux contributions started showing poorer predictions,

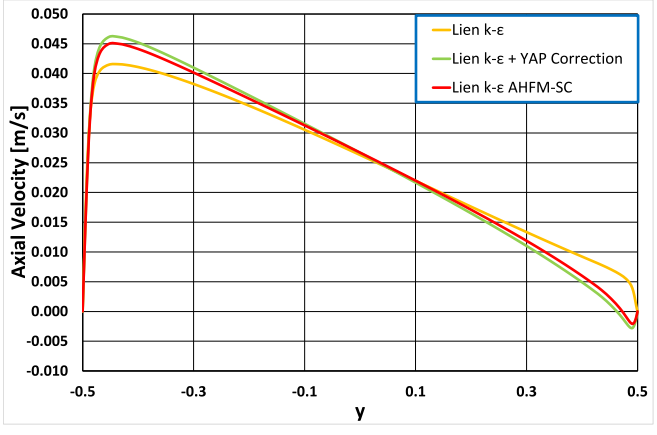

Fig. 15. RANS dimensional velocity distributions for the Ri = 1.00 Case.

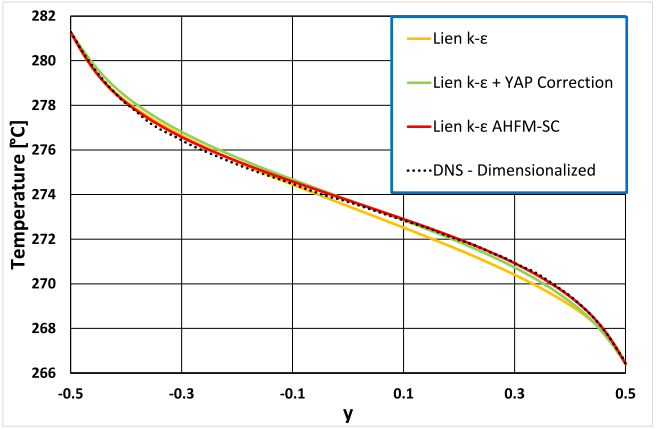

Fig. 16. DNS and RANS dimensional temperature distributions for the Ri = 1.00 Case.

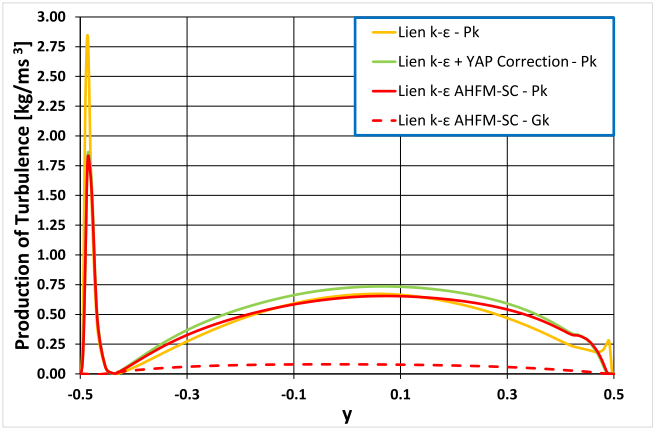

Fig. 17. RANS dimensional turbulence production terms distributions for the Ri = 1.00 Case.

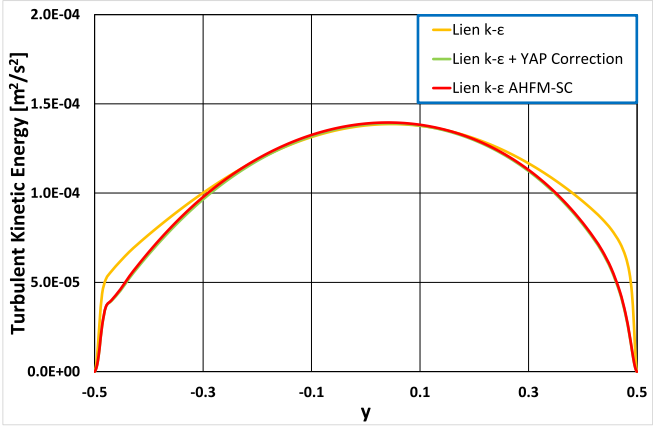

Fig. 18. RANS dimensional turbulent kinetic energy distributions for the Ri = 1.00 Case.

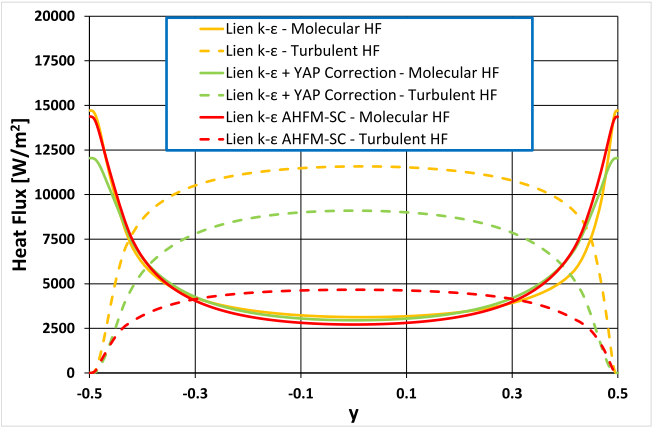

Fig. 19. RANS dimensional heat fluxes distributions along the y-direction for the Ri = 1.00 Case.

which worsened with the increase of the considered Richardson number. Among the relevant limitations reported by these models, the prediction of the velocity distribution, especially for the opposing flow side, and the incapability to capture the DNS temperature trends and reproduce its typical symmetrical profile. On the other hand, the AHFM-SC model provided very good estimations of the DNS data for all the addressed conditions. While some discrepancies can be spotted for the velocity fields, the temperature fields were excellently reproduced, achieving superimposition for several locations. The analysis of the error distribution on the thermal field highlighted the superior capabilities of the AHFM-SC model, which consistently reported the smallest error range.

The performed analyses thus highlight that once buoyancy forces become sufficiently strong, the commonly adopted simple gradient approach is no more a sufficiently good estimation for the turbulent heat flux contributions. Advanced models are thus to be adopted; the presently considered AHFM-SC model proved to be a very good candidate for reporting solid predicting capabilities in all the addressed cases. Future works will keep focusing on the AHFM-SC model, trying to widen the range of applications for which the model achieved validation. Once the model will be validated for several fundamental flow and heat transfer conditions, its capabilities in dealing with real-life industrial and engineering applications involving liquid metal flows will be investigated.

Declaration of Competing Interest

The authors declare that they have no known competing financial interests or personal relationships that could have appeared to influence the work reported in this paper.

Data availability

Data will be made available on request.

References

Bartosiewicz, Y., 2021. High fidelity simulations in support to assess and improve RANS for modeling turbulent heat transfer in liquid metals: the case of forced convection. Nucl. Eng. Des. 382, 111362.
Buzzi, F., Pucciarelli, A., Galleni, F., Tarantino, M., Forgione, N., 2020. Analysis of thermal stratification phenomena in the CIRCE-HERO facility. Ann. Nucl. Energy 131, 107320.
De Santis, D., De Santis, A., Shams, A., Kwiatkowski, T., 2018. The influence of low Prandtl numbers on the turbulent mixed convection in an horizontal channel flow: DNS and assessment of RANS turbulence models. Int. J. Heat Mass Trans. 127 Part C, 345–358.
Durbin, P.A., 1996. On the k-e stagnation point anomaly. Int. J. Heat Fluid Flow 17, 89–90.
Galleni, F., Barone, G., Martelli, D., Pucciarelli, A., Lorusso, P., Tarantino, M., Forgione, N., 2020. Simulation of operational conditions of HX-HERO in the CIRCE facility with CFD/STH coupled codes Nucl. Eng. Des. 361, 110552 https://doi.org/10.1016/j.nucengdes.2020.110552.
GIF portal, https://www.gen-4.org/gif/.
Guo, W., Prasser, H.M., 2022. Direct numerical simulation of turbulent heat transfer in liquid metals in buoyancy-affected vertical channel. Int. J. Heat Mass Transf. 194, 123013.
Guo, W., Shams, A., Sato, Y., Niceno, B., 2020. Influence of buoyancy in a mixed convection liquid metal flow for a horizontal channel configuration. Int. J. Heat Fluid Flow 85, 108630.
Hanjalic, K., Kenjeres, S., Durst, F., 1996. Natural convection in partitioned two-dimensional enclosures at higher Rayleigh numbers. Int. J. Heat Mass Transfer 39 (7), 1407–1427.
Kenjeres, S., Gunarjo, S.B., Hanjalić, K., 2005. Contribution to elliptic relaxation ofturbulent and natural mixed convection. Int. J. Heat Fluid Flow 26, 569–586.
Launder, B.E., 1988. On the computation of convective heat transfer in complex turbulent flows, J. Heat Transf. 110/1113.
Lien, F.S., Chen, W.L., Leschziner, M.A., 1996, Low-Reynolds number eddy viscosity modelling based on non-linear stress-strain/vorticity relations, In: Proceedings of the 3rd Symposium on Engineering Turbulence Modelling and Measurements, 27–29, Crete, Greece.
Marocco, L., Garita, F., 2018. Large eddy simulation of liquid metal turbulent mixed convection in a vertical concentric annulus. J. Heat Transfer 140. https://doi.org/10.1115/1.4038858.
Menter, F.R., 1994. Two-equation eddy-viscosity turbulence modelling for engineering applications. AIAA J. 32 (8), 1598–1605.
MYRTE, http://myrte.sckcen.be/.
NEA, 2015, Nuclear Energy Agency, Handbook on Lead-bismuth Eutectic Alloy and Lead Properties, Materials Compatibility, Thermalhydraulics and Technologies, NEA No. 7268 © OECD 2015.
PATRICIA, https://patricia-h2020.eu/.ss.
Pucciarelli, A., Ambrosini, W., 2018. Use of AHFM for simulating heat transfer to supercritical fluids: application to carbon dioxide data. Int. J. Heat Mass Transf. 127, 1138–1146.
Pucciarelli, A., 2021, Results of a LES application to LBE turbulent flow in a wire-wrapped single rod channel, International Conference on Nuclear Engineering, Proceedings, ICONE, 2021, 3, V003T08A003.
Roelofs, F., 2019. Thermal Hydraulics Aspects of Liquid Metal Cooled Nuclear Reactors, Woodhead Publishing Series in Energy. ISBN 978-0-08-101980-1, 2019.
SESAME, http://sesame-h2020.eu/.
Shams, A., 2018. Towards the accurate numerical prediction of thermal hydraulic phenomena in corium pools. Ann. Nucl. Energy 117, 234–246.
Shams, A., De Santis, A., 2019. Towards the accurate prediction of the turbulent flow and heat transfer in low-prandtl fluids. Int. J. Heat Mass Transfer 130, 290–303.
Shams, A., Roelofs, F., Baglietto, E., Lardeau, S., Kenjeres, S., 2014. Assessment andcalibration of an algebraic turbulent heat flux model for low-Prandtl fluids. Int. J. Heat Mass Transf. 79, 589–601.
Shams, A., Mikuz, B., Roelofs, F., 2018. Numerical prediction of flow and heat transfer in a loosely spaced bare rod bundle. Int. J. Heat Fluid Flow 73, 42–62.
Shams, A., Roelofs, F., Niceno, B., Guo, W., Angeli, D., Stalio, E., Fregni, A., Duponcheel, M., Bartosiewicz, Y., Tiselj, I., Oder, J., 2019a. Reference numerical database for turbulent flow and heat transfer in liquid metals. Nucl. Eng. Des. 353, 110274.
Shams, A., De Santis, A., Koloszar, L.K., Ortiz, A.V., Narayanan, C., 2019b. Status and perspectives of turbulent heat transfer modelling in low-Prandtl number fluids. Nucl. Eng. Des. 353, 110220.
Shams, A., De Santis, D., Padee, A., Wasiuk, P., Jarosiewicz, T., Kwiatkowski, T., Potempski, S., 2020. High-performance computing for nuclear reactor design and safety applications. Nucl. Technol. 206, 283–295.
Shams, A., 2023. Understanding the need for proper turbulent heat flux modelling for non-unity Prandtl number fluids. Computational Fluid Dynamics for Nuclear Reactor Safety (CFD4NRS-9), 20-12 February, College Station, USA.
Shams, A., 2019, Turbulent heat transport. In: Thermal Hydraulics Aspects of Liquid Metal Cooled Nuclear Reactors, Woodhead Publishing, pp. 273–292.
Simcenter STAR-CCM+®, Documentation, Version 13.06. ©2018 Siemens PLM Software.
THINS, https://cordis.europa.eu/project/id/249337/reporting.
Tiselj, I., Cizelj, L., 2012. DNS of turbulent channel flow with conjugate heat transfer at Prandtl number 0.01. Nucl. Eng. Des. 253, 153–160.
Yap, C., 1987. Turbulent heat and momentum transfer in recirculating and impinging flows. Faculty of Technology, University of Manchester, U.K. Ph.D. Thesis.
Zhang, G., Zhang, H., Gu, H., Yang, Y.H., Cheng, X., 2012. Experimental and numericalinvestigation of turbulent convective heat transfer deterioration of supercriticalwater in vertical tube. Nucl. Eng. Des. 248, 226–237.